SIAM J. SCI. COMPUT.
Vol. 25, No. 3, pp. 995–1017

COMPARISON OF SEVERAL DIFFERENCE SCHEMES ON 1D AND 2D TEST PROBLEMS FOR THE EULER EQUATIONS*

RICHARD LISKA† AND BURTON WENDROFF‡

Abstract. The results of computations with eight explicit finite difference schemes on a suite of one-dimensional and two-dimensional test problems for the Euler equations are presented in various formats. Both dimensionally split and two-dimensional schemes are represented, as are central and upwind-biased methods, and all are at least second-order accurate.

Key words. Euler equations, Riemann problems, finite difference schemes, splitting

AMS subject classifications. 35L65, 65M06

DOI. 10.1137/S1064827502402120

1. Introduction.

Hyperbolic conservation laws, and the Euler equations of compressible fluid dynamics in particular, have been the subject of intensive research for at least the past five decades, and with good reason. Their applications are many: aircraft design, stellar formation, and weather prediction, to name only a few. For some theoretical results see [46, 9, 10], and we strongly recommend the preprint server website [14] which contains many papers on theoretical and numerical aspects of hyperbolic conservation laws. Even if the theory were perfect, the applications would not be possible without methods for obtaining approximate solutions. The unfortunate situation here is that rigorous error estimates for supposedly approximate solutions are almost entirely nonexistent, but see [21] for a modest beginning. So, it is universally recognized that tests of methods on difficult problems are essential.

Invariably, any published proposal for a new numerical method will include some actual calculations, and these are clearly too numerous for us to catalogue. The book by Roache [41] contains many early references, and the many fine texts now available (for example, [26, 24]) also contain references to calculations. Our concern here is to compare the behaviors of several methods on problems that seem to us to be sufficiently difficult and representative, thus enabling the reader to draw some conclusions about the applicability of these methods. The now classic work of this nature is the paper by Sod [47]. It showed the shortcomings of schemes such as Lax–Wendroff and Lax–Friedrichs and was very influential in the development of new methods. The one-dimensional (1D) Riemann problem used by Sod in his tests is widely known as Sod's problem. Although it does show the ability of a method to resolve a rarefaction, a contact, and a shock, these waves in Sod's problem are not

*Received by the editors September 16, 2002; accepted for publication (in revised form) April 30, 2003; published electronically November 21, 2003. A preliminary version of this paper appeared in the book of abstracts of Hyp 2002, The Ninth International Conference on Hyperbolic Problems: Theory, Numerics and Applications, T. Hou and E. Tadmor, eds., Caltech, Pasadena, CA, 2002, pp. 213–215. This research was supported by the U. S. Department of Energy under contract W-7405-ENG-36.

http://www.siam.org/journals/sisc/25-3/40212.html

†Faculty of Nuclear Sciences and Physical Engineering, Czech Technical University in Prague, Břehová 7, 115 19 Prague 1, Czech Republic (liska@siduri.fjfi.cvut.cz, http://www-troja.fjfi.cvut.cz/~liska). This author was supported in part by the Czech Grant Agency grant 201/00/0586.

‡Group T-7, Los Alamos National Laboratory, Los Alamos, NM 87544 (bbw@lanl.gov, http://math.unm.edu/~bbw).

particularly strong.

A more difficult set of 1D problems has been considered by Toro [50], who describes in detail several popular methods and shows their behavior on his tests, all of which have easily computed exact solutions. We have included five of Toro's test problems, but we have gone beyond those to include some interesting two-dimensional (2D) tests, including one from [50]. In so doing, however, except in a few cases, we no longer have exact solutions available, so a definitive objective evaluation of the validity of the solutions obtained is not possible. Although the test cases chosen are certainly complex, there are others that would show the need to accurately resolve both smooth and discontinuous structures; therefore we have included the 1D shock entropy wave interaction problem of Shu and Osher [44].

We focus on finite difference methods. Other numerical methods for the Euler equations, such as Lagrangian methods (e.g., [6]), finite element–based methods (e.g., [34]), or relaxation methods (e.g., [20]), are not considered.

Outline. A detailed self-contained discussion of the eight schemes we have chosen would be impractical for this already rather large report; therefore in the next section we present very briefly only the basic ideas and references. Following that are three groups of tests. The first group consists of seven 1D Riemann problems plus the Woodward–Collela blast wave problem. The second group contains six 2D Riemann problems. The third group includes several 2D problems with unstable interfaces: one with an infinite strength shock, one with smooth solution, and two with nonsmooth continuous solution. For each group the data are given, and then for each test in a group the output of some of the eight methods is collected. We also include some comments about the behavior of the various schemes. In those cases for which we do not have the exact solution, the comments are highly subjective.

Disclaimer. Modifications had to be made to fit the various codes into our data structure. Bugs are always a possibility in that case, so we cannot guarantee that all schemes are functioning exactly as intended by their creators.

2. Finite difference schemes. Here we provide a short summary and references for all schemes used in this comparision project. We have chosen eight methods that we feel are representative of the different basic finite difference approaches to solving hyperbolic conservation laws. All schemes are at least formally second-order accurate; one method, the piecewise parabolic method (PPM), is third-order, and another, the weighted essentially nonoscillatory (WENO), is fifth-order in space, third-order in time, although for the smooth periodic test presented in section 4.1 the latter appears to be fifth-order.

Two of the methods described below are dimensionally split, namely, PPM and Virginia hydrodynamics 1 (VH1). While we have chosen to describe all methods in only the most general terms, it is necessary to expound a bit here on the notion of dimensional splitting. Some have described this technique as ill-advised and inefficient, but we have found just the opposite to be the case, as have its defenders. For a system $u_t + f_x + g_y = 0$ the time step is split into two parts. In the first, the equation $u_t + f_x = 0$ is advanced by a 1D scheme. Then using the updated values as data, the equation $u_t + g_y = 0$ is advanced to complete the time step. Either alternation or symmetrization, as first proposed by Strang [48], is usually used to preserve the accuracy of the second-order 1D method and reduce grid alignment effects. On the other hand, the typical 2D scheme would use difference approximations to f_x and g_y and simultaneously rather than sequentially update the data.

There are several advantages to dimensional splitting. It is very easy to convert a 1D code to a 2D code this way. The stability condition is usually less restrictive, and there are possibly fewer flux evaluations necessary, so that it can be more efficient than a 2D calculation. The big disadvantage is that it is not an option for nonrectangular grids.

2.1. A CFLF hybrid scheme—CFLFh. Hybrid schemes and similar flux-corrected-transport schemes have a long history and are presented very well in [24]. The idea is to create a numerical flux consisting of the average of a diffusive flux such as from Lax–Friedrichs (LF) and an oscillatory flux such as Lax–Wendroff (LW). The weights are chosen so that the scheme is formally second-order accurate but becomes sufficiently dissipative in shocks. We have used the fluxes from the 2D LW and LF versions used in the composite scheme [30] along with the Harten weight [15] which can be found in [24].

2.2. Centered scheme with limiter—JT. This scheme by Jiang and Tadmor [18], which is the 2D successor of the Nessyahu–Tadmor 1D scheme NT [35] (see also [2]), is called a nonoscillatory central scheme. It uses neither dimensional splitting nor eigenvector decomposition nor any overt Riemann solver. It does use discontinuous limited piecewise linear reconstruction from cell averages to get fluxes at cell edges. The code is simple enough that it is presented in Appendix 5 of [18], and we were able to use it as is, making only those modifications necessary to fit it into our data structure.

2.3. Positive scheme—LL. This method, devised by Liu and Lax [33, 25], is based on a theorem of Friedrichs stating roughly that if a finite difference method is a two-level method giving the new value of the solution vector as a linear combination of values at the previous time with coefficients that are positive symmetric matrices adding to the identity (but depending only on the independent variables), then the scheme is L^2 stable. The theorem doesn't apply directly to nonlinear systems; nevertheless Liu and Lax created a positive scheme for the Euler equations. It does require an eigenvector decomposition or limiting. We use the code for this scheme published in [33], which is available electronically.

2.4. Clawpack wave propagation scheme—CLAW. Clawpack is a sophisticated flux splitting scheme developed by LeVeque [28] and based on earlier advection ideas [27]. The source and documentation are available electronically [29]. It has many options for the user such as dimensionally split and nonsplit versions, choices for limiters, etc. We have used the nonsplit version with monotonized centered limiter using the Roe Riemann solver with four waves (separate shear and entropy waves).

2.5. Weighted average flux (WAF) scheme—WAFT. WAF is actually a class of schemes that includes the Roe scheme—a fact communicated to us by Quirk [39, 37]. The flux at the cell boundary is obtained as a spatially weighted average over the states of an approximate Riemann solver. A limiter is employed in the computation of the weights. Different methods are obtained for different solvers and different averaging [49, 50, 4]. We call the version we have used WAFT: it is a 2D nonsplit code given us by Toro and is a part of the Numerica library [51]. This code uses a WAF scheme with HLLC (Harten, Lax, van Leer with contact) approximate Riemann solver using the Rankine–Hugoniot condition for evaluating the middle fluxes, as described in Chapter 10 of [50].

2.6. Weighted essentially nonoscillatory scheme—WENO. WENO schemes [19] are an improvement on the essentially nonoscillatory (ENO) scheme of Harten et al. [16] that had been extended in [45]. Upwind-biased spatial differencing is used that produces high-order accuracy for smooth flows but becomes low-order and dissipative for shocks. We have used the code given to us by Jiang that implements a WENO–LF scheme in the terminology of [19]. The spatially fifth-order accurate WENO procedure is applied to an eigenvector decomposition. The time integration is done by a third-order Runge–Kutta procedure.

2.7. Piecewise parabolic—PPM. The PPM [8] is in the class of higher-order accurate Godunov methods. It uses piecewise parabolic limited reconstruction to obtain states to use in the Riemann problems defining the fluxes. Dimensional splitting is used. We use the free version of PPM available at PPMLib library [53] (core routines are available only as SGI binaries).

2.8. Virginia hydrodynamics 1—VH1. VH1 [5] is a free version of the Lagrangian remap PPM method [8] including force sources and all standard geometries in one, two, and three dimensions. The PPM Lagrangian time step using a Riemann solver is followed by a piecewise parabolic remapping step, which remaps quantities from the moved grid to the original one. Dimensional splitting is used. PPMLib [53] also includes the Lagrangian remap PPM method.

3. 1D tests.

3.1. Description of 1D problems. For 1D tests we have chosen five 1D (in x) Riemann problems from [50], Tests 1, 2, 4, 5, 6, plus four others as follows: Noh, the classical 1D Noh problem [36]; Test 3a, a modification of Test 3 from [50], keeping a stationary contact; *peak*, a hard problem with a strong narrow peak in density found by Kuchařík [22]; the Woodward–Collela blast wave problem [52]; and the Shu–Osher shock entropy wave interaction problem [44]. All the 1D problems except the blast wave and shock entropy wave interaction problems are simple Riemann problems with known exact solutions.

TABLE 3.1
Definition of 1D Riemann problem tests.

Test	ρ_L	u_L	p_L	ρ_R	u_R	p_R	x_0	T
1	1	0.75	1	0.125	0	0.1	0.3	0.2
2	1	-2	0.4	1	2	0.4	0.5	0.15
Noh	1	1	10^{-6}	1	-1	10^{-6}	0.5	1
3a	1	-19.59745	1000	1	-19.59745	0.01	0.8	0.012
4	5.99924	19.5975	460.894	5.99242	-6.19633	46.095	0.4	0.035
5	1.4	0	1	1	0	1	0.5	2
6	1.4	0.1	1	1	0.1	1	0.5	2
peak	0.1261192	8.9047029	782.92899	6.591493	2.2654207	3.1544874	0.5	0.0039

The Riemann problems are on the interval $x \in (0,1)$ (except for *peak* which is computed on $x \in (0.1, 0.6)$) with initial discontinuity at $x_0 \in (0,1)$ solved for time $t \in (0,T)$. The initial conditions are given by a constant left state (ρ_L, u_L, p_L) of density, velocity, and pressure on the interval $x \in (0, x_0)$ and right state (ρ_R, u_R, p_R) on the interval $x \in (x_0, 1)$. Each test is defined by the eight parameters $\rho_L, u_L, p_L, \rho_R, u_R, p_R$, x_0, T. For all 1D Riemann problems the data are given in Table 3.1. The Noh problem uses the gas constant $\gamma = 5/3$, while all other tests use $\gamma = 1.4$. All Riemann problem tests use natural boundary conditions.

The classic Woodward–Collela blast wave problem [52] computes the interaction of waves from two Riemann problems with reflecting boundary conditions. The problem is treated again on the interval $x \in (0, 1)$. Two initial discontinuities are located at $x_1 = 0.1$ and $x_2 = 0.9$. The initial density is one and the velocity is zero everywhere. Initial pressures in three different regions (left p_l, middle p_m, and right p_r) are $(p_l, p_m, p_r) = (1000, 0.01, 100)$. Final time is $T = 0.038$.

The Shu–Osher shock entropy wave interaction problem [44] checks how methods behave on the combination of a smooth solution with a shock wave. It is defined on the interval $x \in (-5, 5)$ with initial discontinuity at $x_0 = -4$. Initial data are close to a Riemann problem. The left state is given by constants $(\rho_l, u_l, p_l) = (3.857143, 2.629369, 10.33333)$, and the right state has smooth density and constant velocity and pressure $(\rho_r, u_r, p_r) = (1 + 0.2\sin(5x), 0, 1)$. Final time is $T = 1.8$.

For the numerical treatment of most test problems we use 100 grid cells, with exceptions being Tests 3a and 4 using 200 cells, *blast* and *shock entropy wave interaction* using 400 cells, and *peak* using 800 cells.

3.2. Errors of the numerical solution. For 1D Riemann problems we can compute their exact solutions and thus are able to compare the errors of their numerical solutions, giving us an objective evaluation of the different numerical methods. Table 3.2 summarizes L_1 relative errors of the numerical solutions of these 1D Riemann problems by different numerical schemes. Errors are listed in percentages. For most tests presented errors are errors in density; however, only for Test 2 do we present errors in internal energy and for *peak* in velocity.

TABLE 3.2
Relative L^1 errors listed as percentages for 1D Riemann problem tests for all eight schemes; fail means that the scheme has failed to compute the given test.

Test	1	2	noh	3a	4	5	6	peak
CFLFh	1.5	10.2	1.9	10.3	2.7	0.7	0.8	1.9
JT	1.3	6.4	1.7	8.1	2.3	0.6	0.6	1.1
LL	1.3	31.3	1.5	5.2	2.4	0.5	0.7	0.8
CLAW	0.8	fail	1.3	3.1	1.7	0	0.4	fail
WAFT	0.7	21.9	2.8	2.6	1.4	0	0.3	1.0
WENO	1.3	23.7	2.0	9.2	2.2	0	0.4	2.4
PPM	0.5	6.3	4.6	9.4	1.1	0	0.1	1.3
VH1	0.9	9.6	1.5	3.7	1.3	0	0.3	0.8

3.3. 1D results. Here we show results of all eight schemes for Test 1 in Figure 3.1, for Test 2 in Figure 3.2, for the Noh problem in Figure 3.3, for the blast wave problem in Figure 3.4, and for the Shu–Osher problem in Figure 3.5. For other tests the results are available electronically [31]. Note that for most problems we present the results for the density. The exception is Test 2 for which we present internal energy.

Test 1. This is Toro's variant of Sod's Riemann problem. It differs from Sod's in that there is a sonic point in the rarefaction. All eight methods resolve the shock very well without oscillation, although LL is more dissipative than the others. PPM is outstanding on the contact, with WAFT not far behind. Many of the schemes tested in [50] develop the so-called sonic glitch in the rarefaction, but this is not present in any of our eight schemes; however, PPM, CLAW, and JT have a dip at the base of the rarefaction wave. CFLFh, JT, and VH1 have variations in flat areas.

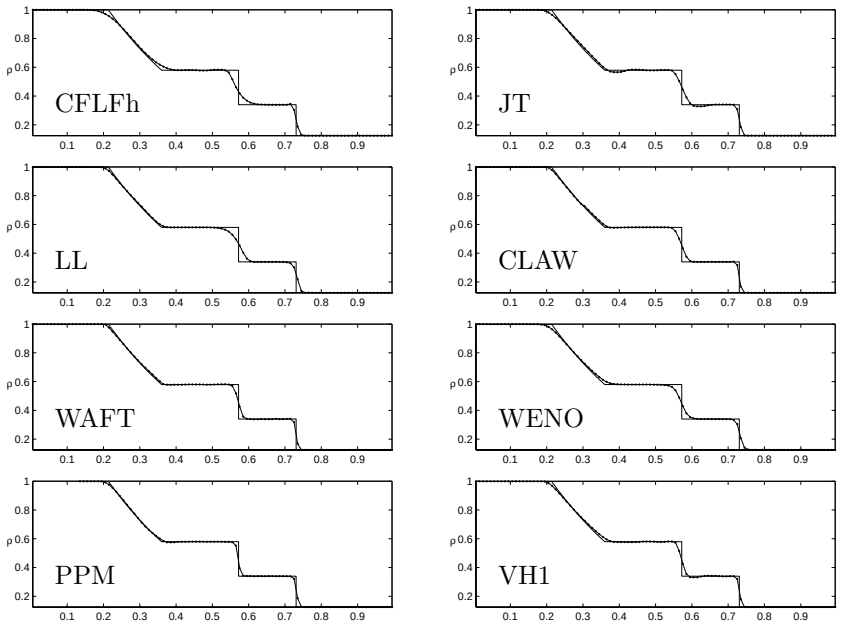

FIG. 3.1. 1*D results (density) for Test* 1 *by all eight schemes.*

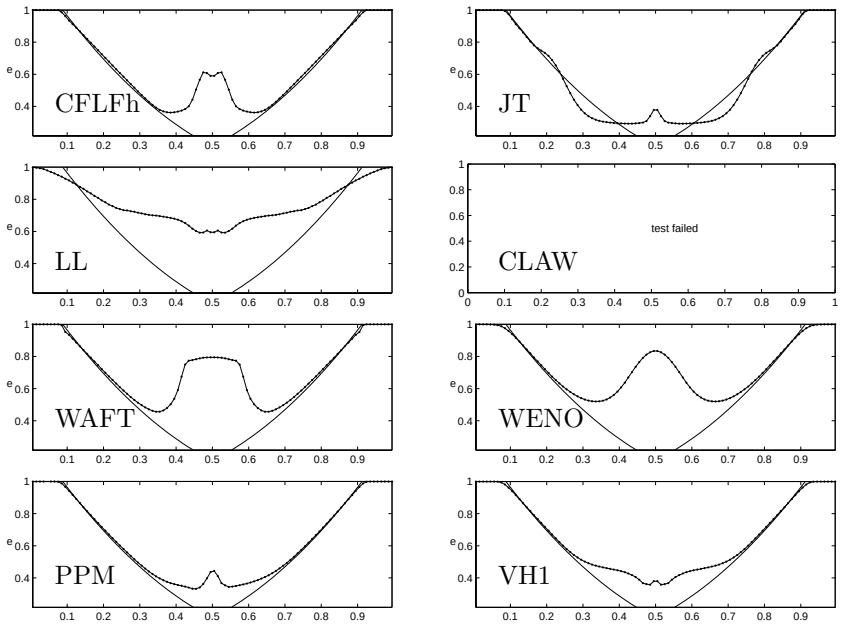

FIG. 3.2. 1*D results (internal energy) for Test* 2 *by all eight schemes.*

Test 2. For this Riemann problem the central state is a near vacuum, in which both ρ and p are close to zero, but the internal energy $e = p/\rho(\gamma - 1)$ is not. It seems that no general Eulerian scheme can compute the internal energy very well. To make LL work for this problem we need to set LL parameters to $\alpha = 0.1$ and $\beta = 2$ on

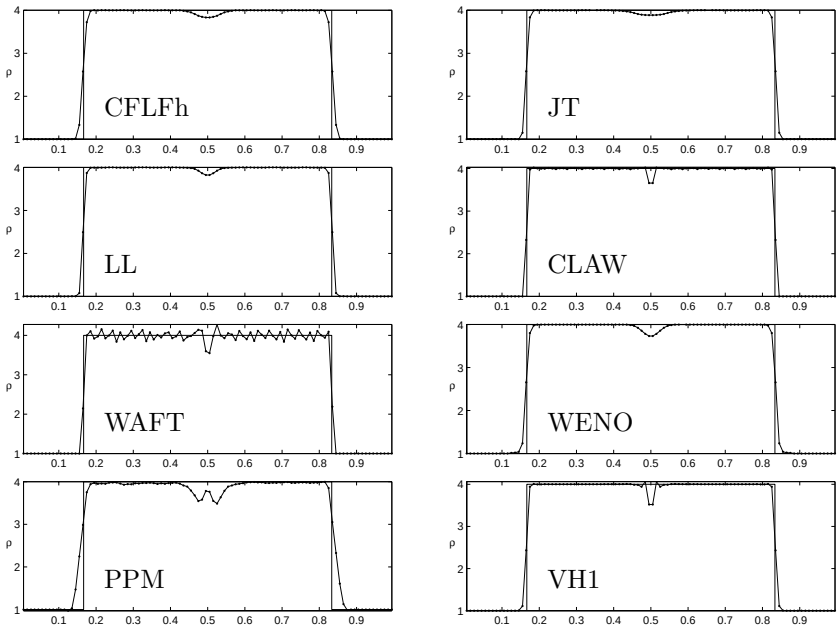

FIG. 3.3. *1D results (density) for the Noh problem by all eight schemes.*

Liu's suggestion [32], which leads to larger viscosity and bad resolution of the heads of rarefaction waves.

1D Noh. The solution of this problem consists of two infinite strength shocks moving out from the center, leaving a constant density and pressure state behind. JT, followed by CFLFh and LL, has the smallest dip in density at the center. PPM has a poorly resolved shock, a significant dip at the center, and is not symmetric about the center. The WAFT run was done with the superbee limiter and is also not symmetric, while a run using a minmod limiter was symmetric; however, this limiter gives worse results than superbee for many other tests. The WAFT result has bad oscillations in a high density area.

Test 3a. In this variant of Toro's Test 3 there is a stationary contact generated at $x = 0.8$. The WAF schemes and CLAW do best, with CFLFh not really acceptable at this resolution.

Test 4. PPM is very good on this problem with two strong shock waves. CLAW and WAFT have good resolution but develop oscillations.

Test 5. This shows which methods (CLAW, WAFT, WENO, PPM, and VH1) are exact for a stationary contact.

Test 6. This is a slowly moving contact. PPM is excellent, followed by WAFT, CLAW, and WENO5. CFLFh develops oscillations behind the contact.

Peak. All schemes have difficulty accurately computing the velocity, especially around the rarefaction with very small change in density. WAFT resolves very nicely the very narrow peak in density between the contact and the shock.

Blast. For this test we present results computed using 400 cells (with "exact" solution from PPM with 2000 cells). The left contact (the first jump from the left around $x = 0.59$) is best resolved by PPM and VH1; however, VH1 is not so good at resolving the right contact (second jump from the right around $x = 0.8$). WAFT is

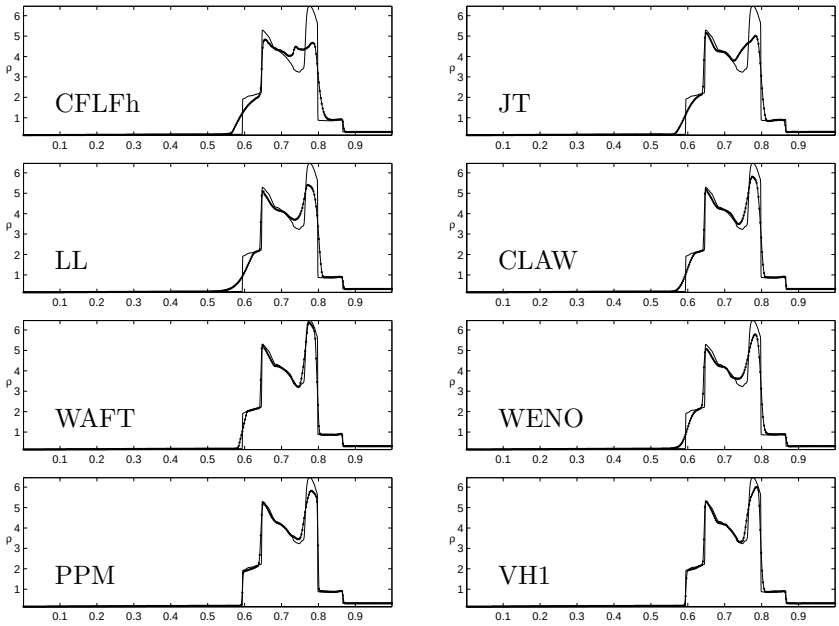

FIG. 3.4. 1*D results (density) for the blast wave by all eight schemes.*

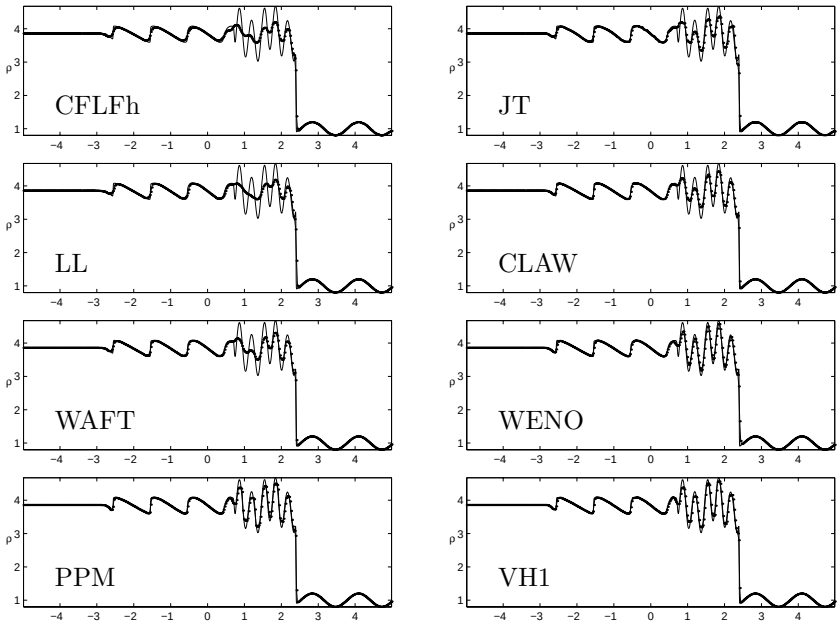

FIG. 3.5. 1*D results (density) for the shock entropy wave interaction by all eight schemes.*

very good at resolving the area around the density maximum.

Shock entropy wave interaction. In this, the Shu–Osher [44] test, pure right-going Mach 3 shock hits entropy sine waves. Presented results use 400 cells, with "exact" solution from WENO having 2000 cells. The key issue here is the resolution

of higher frequency waves behind (on the left of) the shock. WENO, VH1, and PPM are very good. CFLFh and LL are the worst for this test.

4. 2D tests. Due to limited space, we present for some 2D tests (chosen Riemann problems, implosion, and explosion) figures for only six schemes: CFLFh, JT, CLAW, WAFT, WENO, and PPM.

4.1. Accuracy—smooth periodic problem. To check the accuracy of the presented schemes we have computed the numerical solution of an exact smooth solution [19],

$$\rho(x,y,t) = 1 + 0.2\sin(\pi(x+y-t(u+v))), \quad u,v,p \ \text{ constants},$$

of the Euler equations for an ideal gas. We have used the particular values $u = 1, v = -1/2,\ p = 1$ for velocities and pressure. The gas constant is again $\gamma = 1.4$. Periodic boundary conditions are employed. The problem is run on the series of refined grids with $25 \times 25, 50 \times 50, 100 \times 100, 200 \times 200$ cells until the final time $T = 4$ giving the movement of the wave by one full period. Results for all schemes are summarized in Table 4.1 for relative L^1 norm density errors which are shown as percentages. The order of accuracy of schemes in this table is computed as the base 2 logarithm of the ratio of two errors from neighboring columns.

From the table we see that the most accurate scheme is fifth-order WENO followed by third-order PPM. Also, both of these schemes keep the high accuracy from very rough grids. All other schemes are second order.

TABLE 4.1

Relative L^1 density errors shown in percentages for the 2D smooth periodic problem for all eight schemes on a refined grid with orders of accuracy.

Scheme	25	Order	50	Order	100	Order	200
CFLFh	2.5	2.3	$5.1{\cdot}10^{-1}$	2.1	$1.2{\cdot}10^{-1}$	2.0	$3.1{\cdot}10^{-2}$
JT	1.1	2.3	$2.3{\cdot}10^{-1}$	1.9	$5.9{\cdot}10^{-2}$	1.9	$1.6{\cdot}10^{-2}$
LL	2.0	1.3	$8.0{\cdot}10^{-1}$	1.9	$2.1{\cdot}10^{-1}$	2.0	$5.4{\cdot}10^{-2}$
CLAW	$4.1{\cdot}10^{-1}$	2.5	$7.3{\cdot}10^{-2}$	2.2	$1.6{\cdot}10^{-2}$	2.2	$3.7{\cdot}10^{-3}$
WAFT	$5.7{\cdot}10^{-1}$	-0.1	$6.0{\cdot}10^{-1}$	1.4	$2.3{\cdot}10^{-1}$	1.8	$6.7{\cdot}10^{-2}$
WENO	$3.1{\cdot}10^{-2}$	5.0	$9.7{\cdot}10^{-4}$	5.0	$3.1{\cdot}10^{-5}$	4.5	$1.3{\cdot}10^{-6}$
PPM	$2.4{\cdot}10^{-2}$	3.1	$2.8{\cdot}10^{-3}$	3.0	$3.4{\cdot}10^{-4}$	3.0	$4.3{\cdot}10^{-5}$
VH1	$4.5{\cdot}10^{-1}$	2.2	$9.7{\cdot}10^{-2}$	2.4	$1.9{\cdot}10^{-2}$	2.3	$3.9{\cdot}10^{-3}$

4.2. Speed. To compare the speed of the schemes we have measured CPU time (on an SGI Origin with 250 MHz MIPS R10000 processor—we have PPM available only on SGI machines) for all of them for the 2D Riemann problem (Case 4 in section 4.3) on the grid of 400×400 cells up to time $T = 0.05$. The results are summarized in Table 4.2, showing also the ratio of how many times slower the given scheme is than the fastest of our eight schemes (JT) and the number of adaptive time steps used by the different schemes. One can note that four schemes (JT, LL, WENO, and VH1) need about twice as many time steps as the other four schemes. In fact, the other four schemes use a CFL limit of 1, while three schemes (JT, LL, and WENO) need a CFL limit of 1/2 and VH1 uses a CLF limit of 0.6. WENO and LL are slow; all the others are quite fast. It is remarkable that JT is the fastest scheme even though it uses a CFL limit of 1/2, and VH1 with CLF = 0.6 is only a little bit slower. For many schemes we had to manipulate the data to fit into our framework, which might slow down some schemes, so this speed comparison data should be understood as very rough.

TABLE 4.2

Execution CPU times for 2D Riemann problem Case 4 on the grid of 400×400 cells up to time $T = 0.05$. Ratio between the CPU time of the given scheme and that of the fastest scheme (JT). Number of time steps used by each scheme.

Scheme	CPU time[s]	Ratio	Time steps
CFLFh	133	1.3	46
JT	103	1.0	92
LL	310	3.0	88
CLAW	118	1.1	49
WAFT	150	1.5	46
WENO	570	5.5	89
PPM	140	1.4	46
VH1	110	1.1	92

TABLE 4.3

Initial states in four left/right–upper/lower quadrants (for each case, the first row in the table is for two upper quadrants and the second row for two lower ones) for 2D Riemann problems for the pressure p, density ρ, x-component of velocity u, and y-component of velocity v. T is the final time.

Case	Left				Right				T
	p	ρ	u	v	p	ρ	u	v	
	0.3	0.5323	1.206	0.0	1.5	1.5	0.0	0.0	
3	0.029	0.138	1.206	1.206	0.3	0.5323	0.0	1.206	0.3
	0.35	0.5065	0.8939	0.0	1.1	1.1	0.0	0.0	
4	1.1	1.1	0.8939	0.8939	0.35	0.5065	0.0	0.8939	0.25
	1.0	2.0	0.75	0.5	1.0	1.0	0.75	-0.5	
6	1.0	1.0	-0.75	0.5	1.0	3.0	-0.75	-0.5	0.3
	1.0	1.0	0.7276	0.0	0.4	0.5313	0.0	0.0	
12	1.0	0.8	0.0	0.0	1.0	1.0	0.0	0.7276	0.25
	0.4	0.5197	-0.6259	-0.3	1.0	1.0	0.1	-0.3	
15	0.4	0.8	0.1	-0.3	0.4	0.5313	0.1	0.4276	0.2
	1.0	2.0	0.0	-0.3	1.0	1.0	0.0	-0.4	
17	0.4	1.0625	0.0	0.2145	0.4	0.5197	0.0	-1.1259	0.3

4.3. Description of 2D Riemann problems. We have taken six cases from the collection of 2D Riemann problems proposed by [43] and used by others [25, 23], namely, Cases 3, 4, 6, 12, 15, and 17 from [25] (which are configurations $3, 4, B, F, G, K$ from [43]). These problems are solved on the square $(x, y) \in (0, 1) \times (0, 1)$. The square is divided into four quadrants by lines $x = 1/2,\ y = 1/2$. The Riemann problems are defined by initial constant states in each quadrant. These initial states in left/right–upper/lower quadrants for the pressure p, density ρ, x-component of velocity u, and y-component of velocity v are presented in Table 4.3 together with the time T at which the results are presented. All these problems use the gas constant $\gamma = 1.4$. In the figures presenting results we use the same set of contours for density as used in [43]. All the Riemann problems in [43] are proposed in such a way that the solutions of all four 1D Riemann problems between quadrants have exactly one wave (shock, rarefaction, or contact-slip). Following [25], let R stand for rarefaction, S for shock, and J for contact-slip. Starting at the left side and going clockwise, the cases are as follows: **Case 3**: S, S, S, S; **Case 4**: S, S, S, S; **Case 6**: J, J, J, J; **Case 12**: J, S, S, J; **Case 15**: J, R, S, J; **Case 17**: S, J, R, J.

4.4. Results for 2D Riemann problems. As we stated in the introduction, exact solutions are not known for these 2D Riemann problems. Furthermore, the color maps can hide details such as small oscillations. But by having pressure as color and

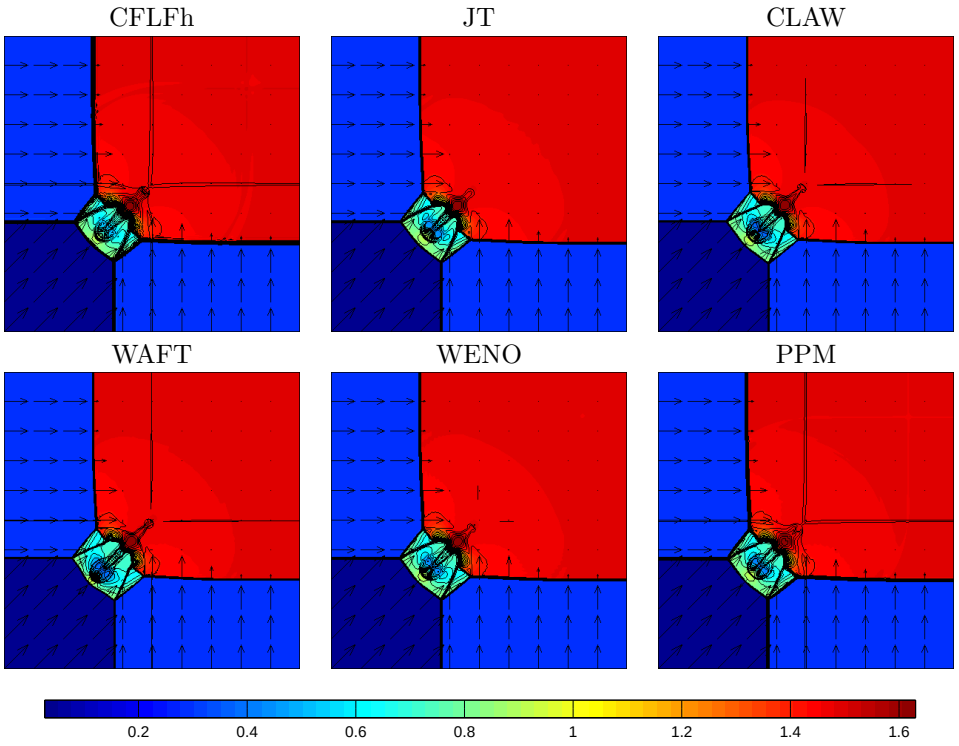

FIG. 4.1. *Results for the 2D Riemann problem Case 3 by six schemes. Pressure is displayed by color, density by 32 contours (from 0.16 to 1.71 with step 0.05), and velocity by arrows. For all cases the computations were done and are presented on the square* $(x, y) \in (0, 1) \times (0, 1)$.

density as contours, it is at least possible to see what the schemes think the structures are. In some cases there are clear errors caused by poor resolution of the initial 1D problems.

Results for Case 3 are shown in Figure 4.1, for Case 12 in Figure 4.2, and for Case 15 in Figure 4.3. For other cases from Table 4.3, results are available electronically [31]. These runs are for grids with 400×400 cells. The color pressure map is overlaid by density contours and velocity arrows.

Case 3. One can notice the different resolution (by different schemes) of the four 1D shocks separating the four regions of constant states. To some extent all schemes agree on the basic structure of the solution in the region where these four shocks interact.

Note the artifacts remaining for some schemes on two segments of the initial discontinuities between the upper right quadrant and upper left and lower right quadrants. When we look at these in more detail we find that these errors are present for all schemes; it is just that for some schemes (CFLFh, CLAW, WAFT, PPM, and VH1) they are large enough so that they are visible in the chosen density contours. Even further, when we try to compute just the 1D Riemann problem defined between the two upper quadrants (or equivalently between the two right quadrants), these artifacts (dip in density) are present for all schemes in the 1D results. Four schemes (CFLFh, WAFT, PPM, and VH1) also show such errors at the other two initial inner jump segments between the lower left quadrant and two of its neighbors on the right

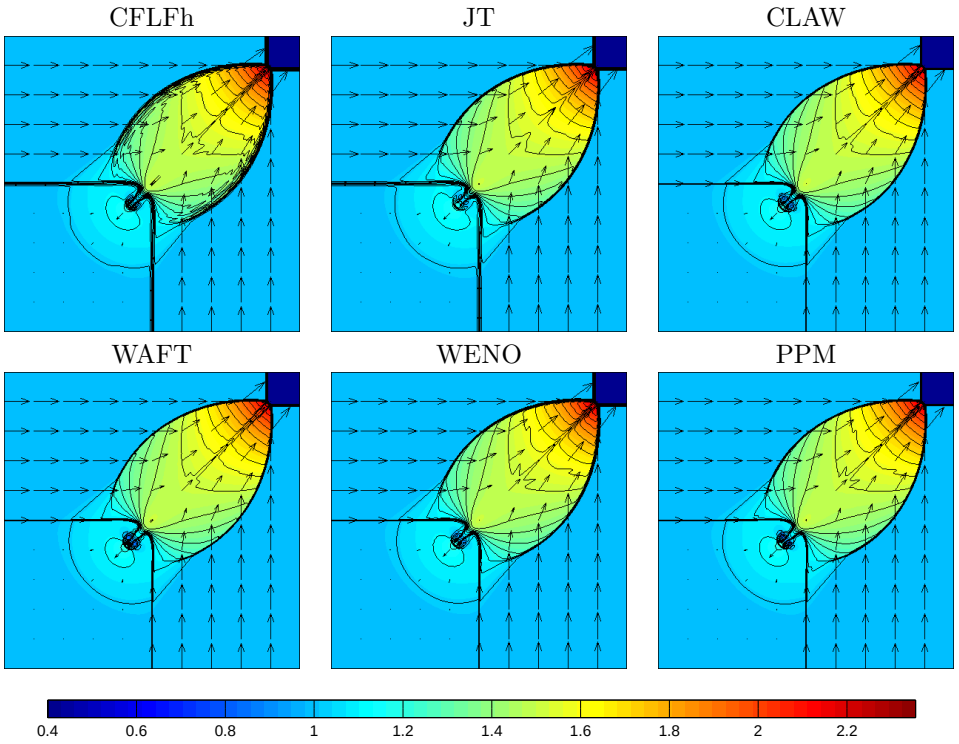

FIG. 4.2. *Results for the* 2*D Riemann problem Case* 12 *by six schemes. Pressure is displayed by color, density by* 30 *contours (from* 0.54 *to* 1.7 *with step* 0.04*), and velocity by arrows. For all cases the computations were done and are presented on the square* $(x, y) \in (0, 1) \times (0, 1)$.

and at the top. This is sometimes the price paid for good contact resolution; there is not enough dissipation to reduce a residual error in density.

Case 4. CFLFh is noisy. The other methods are very similar to each other. Most methods resolve all the shocks well—both the straight 1D shocks separating two constant states and the two curved shocks bordering the lens-shaped region of higher density and pressure. The solution in this region should be symmetric about the lens axis (if we would stay in a coordinate system fixed to this axis, which is moving with constant speed, the problem would be symmetric about this axis). Some schemes do not keep this symmetry in all details; e.g., CFLFh and JT have differences along the upper and lower curved shocks.

Case 6. The contact-resolving ability of WAFT and PPM shows up very well here. All the schemes have grid-aligned artifacts in the high pressure areas around boundaries, which also appear in density. Only for CFLFh do these artifacts also show up on the lower right in the chosen density contour levels. Some of these relics are standing around original jump segments, while the others result from waves emanating from the initial jumps, which are faster than the main contact waves.

Case 12. The key issue here is the resolution of the stationary contacts bordering the lower left quadrant. When we compare these stationary contacts with the 1D Test 5, we see that all schemes which exactly resolve the stationary contact there (CLAW, WAFT, WENO, PPM and VH1) also exactly resolve the stationary contacts here. The data for this problem are symmetric about the (0,0) (1,1) diagonal, and the

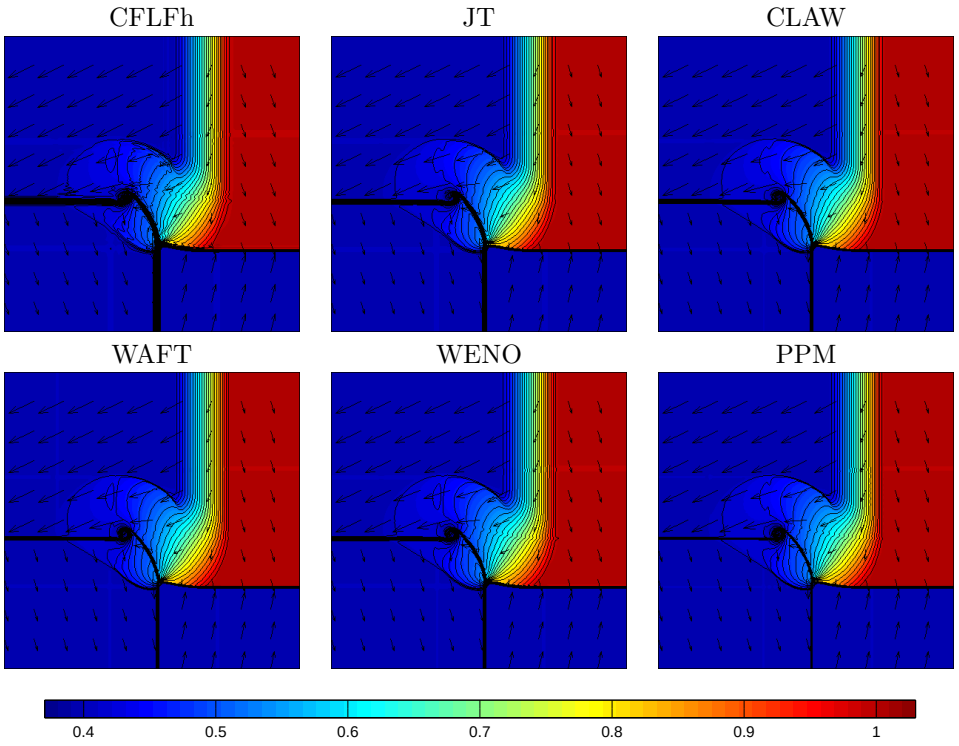

FIG. 4.3. *Results for the 2D Riemann problem Case 15 by six schemes. Pressure is displayed by color, density by 29 contours (from 0.43 to 0.99 with step 0.02), and velocity by arrows. For all cases the computations were done and are presented on the square* $(x, y) \in (0, 1) \times (0, 1)$.

nonsymmetric dimensionally split schemes PPM and VH1 preserve the symmetry quite well, as do all the other nonsplit methods.

Case 15. Resolution of slowly moving contacts bordering the lower left constant state is important here (note the short curved contact in the middle), and one might compare these contacts with 1D Test 6. As in Case 6, a detailed inspection reveals errors aligned with the slip and shock lines that show up in the pressure color map. As in Case 6, these artifacts appear also in density, but they are not visible with the chosen density contour levels, and they have the same origin as in Case 6.

Case 17. Here we have an interesting disagreement. LL shows a possible instability on the lower slip line not seen by the others. As in Case 12, the resolution of two standing contacts on the line $x = 1/2$ is important, and we can again compare these contacts with 1D Test 5.

4.5. Noh problem. This is a classic test of Noh [36] for an ideal gas with $\gamma = 5/3$ for which there is an exact solution. The initial density is 1, the initial pressure is 0 (we set initial pressure to 10^{-6} in the numerics, as many schemes cannot deal with zero pressure), and the initial velocities are directed toward the origin in the plane with magnitude 1. The solution is an infinite strength circularly symmetric shock reflecting from the origin. Behind the shock (i.e., inside the circle) the density is 16, the velocity is 0, and the pressure is 16/3. The shock speed is 1/3 and ahead of the shock, that is, for $\sqrt{x^2 + y^2} > t/3$, the density is $(1 + t/\sqrt{x^2 + y^2})$, while velocity and pressure remain the same as initially. The computational domain is $0 \le x \le 1$,

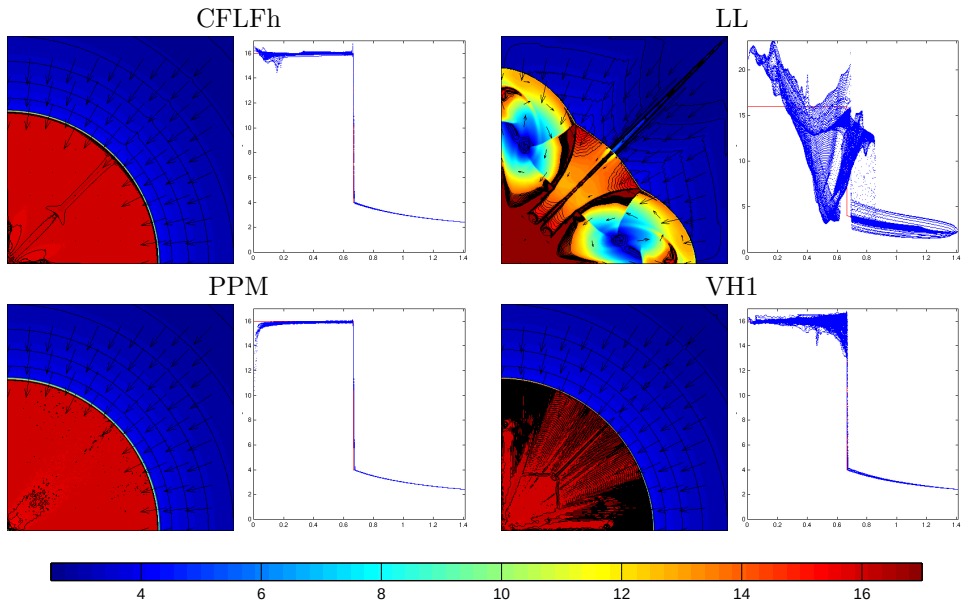

FIG. 4.4. *Results for the Noh problem by the CFLFh, LL, PPM, and VH*1 *schemes. JT, CLAW, WAFT, and WENO have failed for this problem. The density color map is overlaid by* 23 *density contours (from* 2.5 *to* 4 *with step* 0.25 *and from* 14 *to* 17 *with step* 0.2*) and velocity arrows on the left. Scatter plot of density versus radius is on the right. The computations were done on the square* $(x, y) \in (0, 1) \times (0, 1)$ *with* 400×400 *grid to time* $T = 2$.

$0 \le y \le 1$. At the boundaries $x = 1$ and $y = 1$ we used the exact density as a function of time and radius together with the initial pressure and velocity. At the other two boundaries $x = 0$ and $y = 0$ we used the symmetric (reflecting) boundary conditions. This is a difficult problem. The Lagrangian codes dealing with this problem suffer from a very large error in the density at the center. For an analysis of this problem see [40].

Results of the Noh problem on the 400×400 grid are shown in Figure 4.4. The schemes JT, CLAW, WAFT, WENO, for which no result is shown, failed to run. JT ran on a 100×100 grid but not on the 400×400 grid. PPM required a CFL limit of 0.2 for the 400×400 grid, but ran with CFL $= 0.8$ for a 100×100 grid. LL was completely wrong, and we also ran it on the whole plane to be certain that this was not the result of some error on the symmetry boundary. VH1 is very oscillatory, PPM is good; however, we have to use CFL $= 0.2$. CFLFh is reasonably good.

4.6. Rayleigh–Taylor instability. Rayleigh–Taylor instability is a physical phenomenon appearing when a layer of heavier fluid is placed on top of a layer of lighter fluid. For this problem we include a gravitational source term in the momentum equation. We treat this problem in the region $(x, y) \in (0, 1/6) \times (0, 1)$ with the gravitational acceleration $g = 0.1$ in the $-y$ direction. The upper fluid has density 2 and the lower fluid 1. The interface of the fluids is at $y = 1/2 + 0.01 \cos(6\pi x)$, i.e., a slightly perturbed line $y = 1/2$. The initial pressure is hydrostatic and the fluids are initially at rest. Around the interface the initial conditions are smoothed out. Boundary conditions on all four border lines are reflecting.

These runs are for a grid of 100×400 cells on half of the mushroom and are shown

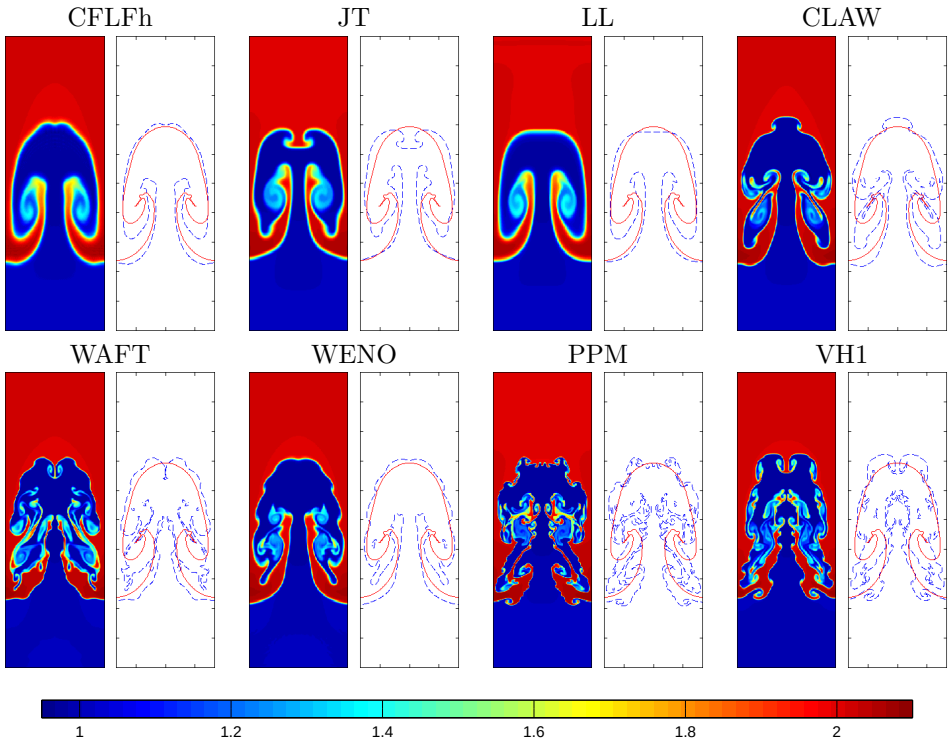

FIG. 4.5. *Results for the Rayleigh–Taylor problem by all eight schemes. Shown are the density color map and front contour. The solid line in the contour plots is the result of a front tracking code. The computations were done on the rectangle* $(x, y) \in (0, 1/6) \times (0, 1)$ *with* 100×400 *grid to time* $T = 8.5$.

in Figure 4.5. The density color map and density contour are shown separately. The solid line in the contour plot was provided by Grove and Mousseau of Los Alamos [13] and is the result of a front tracking code, while the dashed line is the density $\rho = 1.5$ contour. The interface between the light and heavy fluid is unstable. As might be expected, the less dissipative schemes such as CLAW and WENO show this interface breaking up, while the more dissipative schemes like CFLFh suppress the instability. Aslam [3] has reported to us that the interface breaks up very early with a very high resolution fine grid WENO scheme. The front tracking contour also seems to suppress the instability.

4.7. Implosion problem. This converging shock problem was presented in [17]. In [7] several variants of this problem, including other shapes of interior low density and low pressure region, were treated. The gas is placed in a square box. Inside a smaller square positioned at the center of the box and rotated by $\pi/4$ (see Figure 4.6 (a)) the gas has initially smaller density and pressure than in the rest of the box. As in [17] we use the box $(x, y) \in (-0.3, 0.3) \times (-0.3, 0.3)$ and the smaller square with corners at $(\pm 0.15, 0), (0, \pm 0.15)$. The computation is done only in the upper right quadrant $(x, y) \in (0, 0.3) \times (0, 0.3)$ of the box with diamond corners at points $(0.15, 0), (0, 0.15)$. Initial data inside the diamond are $\rho_i = 0.125$, $p_i = 0.14$ and outside are $\rho_o = 1$, $p_o = 1$. Initial velocities are zero. The gas constant is $\gamma = 1.4$. Reflecting boundary conditions are used on all four boundaries. The initial data are the Sod problem data [47].

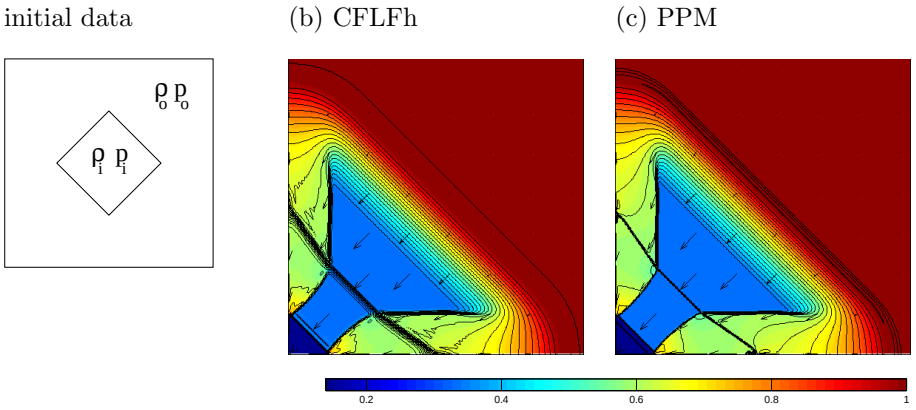

FIG. 4.6. *Initial data of the implosion problem* (a) *and results at an early stage by CFLFh* (b) *and PPM* (c) *schemes on the upper right quadrant. The color pressure map is overlaid by* 36 *density contours (from* 0.125 *to* 1 *with step* 0.025*) and velocity arrows. The computations were done on the square* $(x, y) \in (0, 0.3) \times (0, 0.3)$ *with* 400×400 *grid to time* $T = 0.045$ *and are presented on the square* $(0, 0.22) \times (0, 0.22)$.

First we present in Figure 4.6 results by CFLFh and PPM (as worst and best, respectively) schemes at the early stage at time $T = 0.045$. There is a clear consensus among the codes for the very early stages of the evolution. The initial interior diamond boundary is a contact discontinuity that is nicely resolved by PPM and WAFT but rather badly resolved by CFLFh. The color pressure map shows that the pressure is continuous normal to the contact but also that there is a pressure discontinuity tangential to the contact. The animation on the website [31] is particularly effective in showing the wave structure.

Figure 4.7 shows results at a late stage at time $T = 2.5$ by CLAW, WENO, WAFT, and PPM schemes. In the later stages there is also a consensus on the gross structure of the waves reflected fromn the boundary. The fate of the initial contact discontinuity is not clear, but there is remarkable agreement between CLAW and WENO that a jet has formed. We can also see here the lack of symmetry in the split dimension PPM and VH1, which both use alternating Strang splitting, as well as in the 2D code WAFT using a superbee limiter (with a minmod limiter, WAFT keeps symmetry).

4.8. Explosion. The explosion problem proposed in [50] is a circularly symmetric 2D problem with initial circular region of higher density and higher pressure. In particular we set the center of the circle to the origin, its radius to 0.4, and compute on a quadrant $(x, y) \in (0, 1.5) \times (0, 1.5)$. Density and pressure are $\rho_i = 1$, $p_i = 1$ inside the circle and $\rho_o = 0.125$, $p_o = 0.1$ outside. The gas is initially at rest and its gas constant is $\gamma = 1.4$. This problem (evolution of unstable contact at later times) is sensitive to perturbations of the interface and, as noted in [50], for the cells which are crossed by the initial interface circle one needs to use area-weighted initial density and pressure. Nevertheless it appears that an instability develops. There is a shock reflecting from the center that passes through the contact and seems to have no effect.

Figure 4.8 shows results by CFLFh, JT, CLAW, WAFT, WENO, and PPM schemes. Higher-order schemes WENO and PPM are more sensitive to interface instability than the lower-order schemes CLAW and WAFT. The narrowest contact interface is resolved by WAFT. The interface is rather poorly resolved by CFLFh and

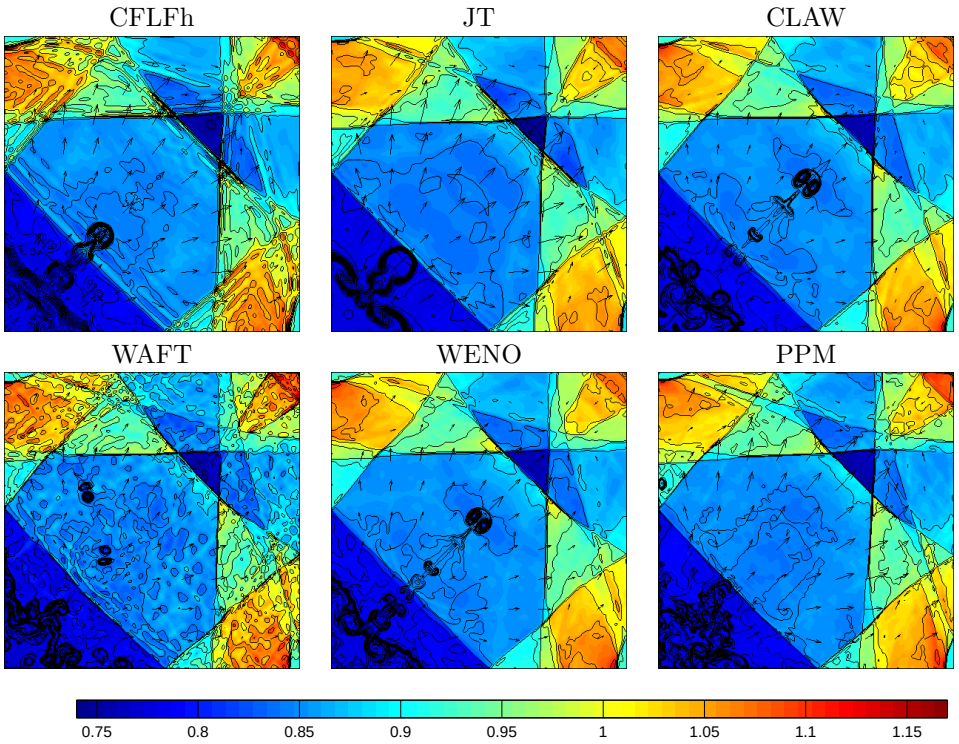

FIG. 4.7. *Results for the implosion problem at a late stage by six schemes. The color pressure map is overlaid by* 31 *density contours (from* 0.35 *to* 1.1 *with step* 0.025*) and velocity arrows. The computations were done on the square* $(x, y) \in (0, 0.3) \times (0, 0.3)$ *with* 400×400 *grid to time* $T = 2.5$.

TABLE 4.4
Maximum errors in y velocity for the odd-even problem.

Schemes	$\max(\lvert u_y \rvert)$
CFLFh, LL, WENO	0
JT	$2{\cdot}10^{-20}$
CLAW	$1{\cdot}10^{-16}$
WAFT	$5{\cdot}10^{-4}$
PPM	$3{\cdot}10^{-7}$
VH1	$1{\cdot}10^{-1}$

LL. There are numerical boundary effects at the upper right corner that we were not able to eliminate. These runs below are for grids 400×400 cells at time $T = 3.2$. A color pressure map is overlaid by density contours and velocity arrows.

4.9. Odd-even decoupling. Here we treat a problem similar to Quirks's odd-even decoupling problem from [38]; for recent analysis of this problem, see [12]. As most of our schemes work on rectangular grids only, we cannot use Quirks's formulation with a perturbed grid. Instead we use the problem setup suggested to us by Abouziarov [1]: the Woodward–Colella 1D blast wave problem described in section 3.1 is solved on a rectangle $(x, y) \in (0, 1) \times (0, 0125)$ with initial data independent of y (and zero velocity in the y direction) on the 800×10 grid. The boundary conditions are reflective in x direction and periodic in the y direction, and the problem is run as in one dimension until time $T = 0.038$.

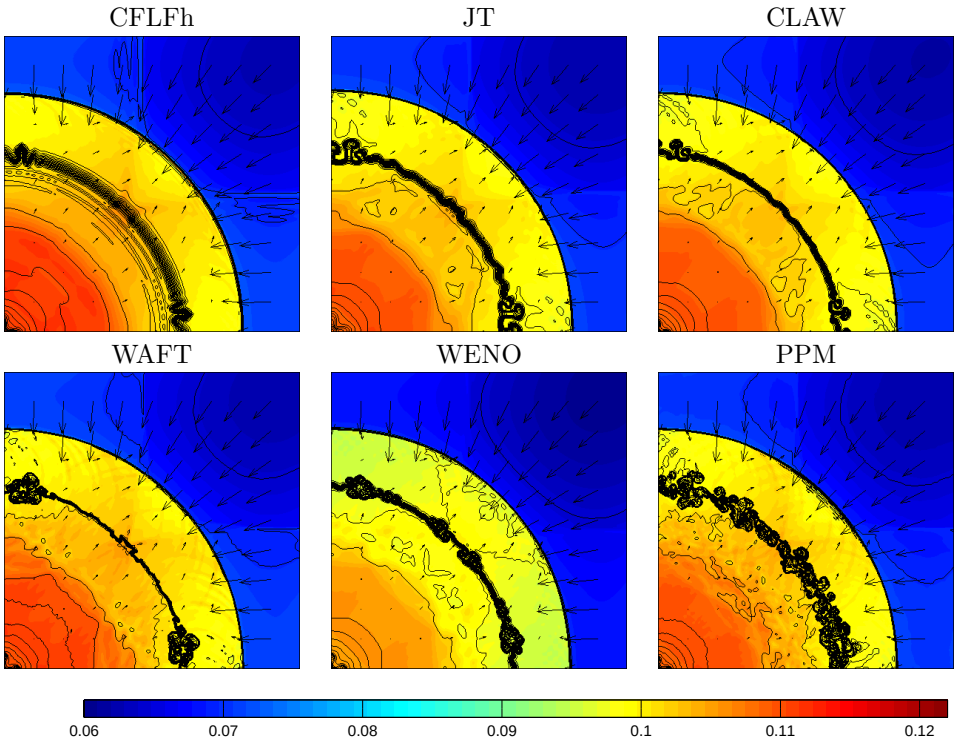

FIG. 4.8. *Results for the explosion problem by six schemes. The color pressure map is overlaid by* 27 *density contours (from* 0.08 *to* 0.21 *with step* 0.005*) and velocity arrows. Computations were done on the square* $(x, y) \in (0, 1.5) \times (0, 1.5)$ *with* 400×400 *grid to time* $T = 3.2$.

The numerical solution should remain independent of y; however, two of our schemes, namely VH1 and WAFT, develop pathological behavior starting with small nonzero y velocity which varies in the y direction, amplifies as an instability, and also influences the density. In Table 4.4 we present the maximum deviation of the y velocity from zero at the final time. The error in the y velocity is zero for CFLFh, LL, and WENO. It is very small for JT and CLAW for which it does not depend on y and does not grow further for longer time. For PPM the y velocity error at this time is small and does not influence the density; however, this error depends on y and grows with time; e.g., for double time $T = 0.076$ it reaches 10^{-5} and still does not influence the density, but eventually at later times it will influence the whole solution. For VH1 and WAFT the error in y velocity is big and also influences the density, as we can see in Figure 4.9 presenting a critical part of the solution where oscillations appear.

4.10. Gresho problem. The Gresho problem [11, 42] is a rotating vortex problem independent of time. Angular velocity depends only on radius, and the centrifugal force is balanced by the pressure gradient

$$u_\phi(r) = \begin{cases} 5r & \\ 2 - 5r, & \\ 0 & \end{cases} \qquad p(r) = \begin{cases} 5 + \frac{25}{2} r^2, & 0 \le r < 0.2, \\ 9 - 4\ln 0.2 + \frac{25}{2} r^2 - 20r + 4\ln r, & 0.2 \le r < 0.4, \\ 3 + 4\ln 2, & 0.4 \le r. \end{cases}$$

The radial velocity is zero and the density is one everywhere. The Gresho problem has been used in [11, 42] for incompressible flow; here we apply it to the Euler equations.

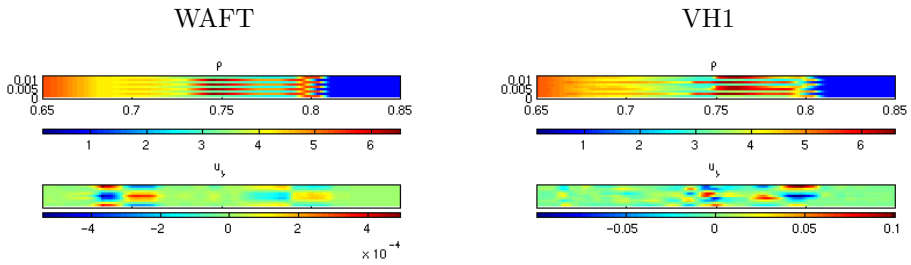

FIG. 4.9. *Density (up) and y velocity (down) profile for odd-even decoupling problem in critical area* $(x, y) \in (0.65, 0.85) \times (0, 0125)$ *for the WAFT and VH*1 *schemes.*

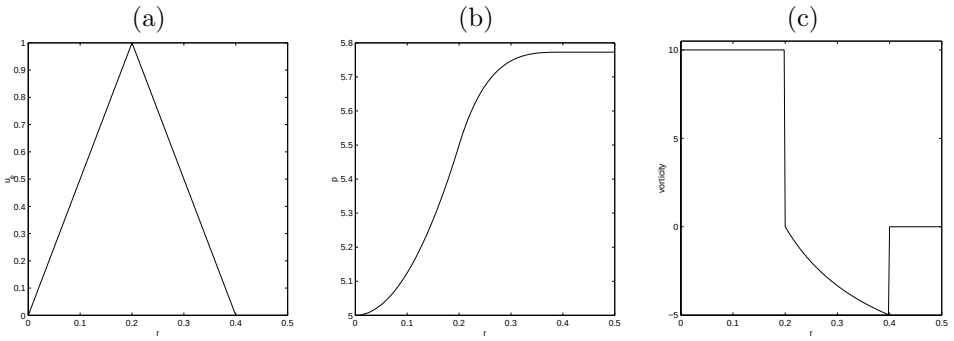

FIG. 4.10. *Exact solution of the Gresho problem: dependence of angular velocity* (a), *pressure* (b), *and vorticity* (c) *on radius.*

Pressure has a minimum in the center and can be shifted by a constant value. Here we use higher pressure $p(0) = 5$ in the center. The vorticity of the solution is 10 for $0 \le r < 0.2$, $2/r - 10$ for $0.2 \le r < 0.4$, and zero for $0.4 \le r$. The dependence of angular velocity, pressure, and vorticity on radius is plotted in Figure 4.10.

We have solved this problem on a rectangle $(x, y) \in (0, 1) \times (0, 1)$ with transmissive boundary conditions until time $T = 3$ on 20×20 and 40×40 grids. We use such rough grids to be comparable with [11, 42] using a 20×20 grid. Table 4.5 summarizes the relative L^1 errors of vorticity and density and the relative error of total kinetic energy. Errors are shown in percentages. From errors in Table 4.5 CFLFh looks best on the 20×20 grid; however, its results are not improved on the finer 40×40 grid, and it oscillates on this grid. PPM and VH1 are very good and converge, and JT and LL are the worst for this problem.

The moving Gresho problem is the same problem as the Gresho problem, but with the vortex convected by velocity one in the x direction, so the initial conditions are the same with the x velocity component increased by one. We have solved this problem on a rectangle $(x, y) \in (0, 4) \times (0, 1)$ with transmissive boundary conditions until time $T = 3$ on 80×20 and 160×40 grids. Table 4.6 summarizes the relative L^1 errors of vorticity and density and the relative error of total kinetic energy. Errors are shown in percentages. Figure 4.11 shows a resulting vortex computed by all schemes on the 160×40 grid. Concerning the vorticity error in Table 4.6, for the 80×20 grid WENO is best; however, this error does not improve much with the finer 160×40 grid, and there is a large error in total kinetic energy on the coarser 80×20 grid which

TABLE 4.5

Relative L^1 errors of vorticity and density shown in percentages and relative error shown in percentages of total kinetic energy (TKE) for the Gresho problem by all eight schemes on 20×20 and 40×40 grids.

	20×20 grid			40×40 grid		
Scheme	L^1 Vorticity error	L^1 Density error	Relative TKE error	L^1 Vorticity error	L^1 Density error	Relative TKE error
CFLFh	22	0.22	0.2	20	0.16	0.4
JT	89	0.56	55.2	45	0.22	18.3
LL	71	2.27	65.6	44	0.23	26.1
CLAW	50	0.33	29.9	28	0.10	6.1
WAFT	47	0.24	7.7	26	0.07	5.7
WENO	38	0.35	30.9	27	0.06	3.7
PPM	25	0.20	9.1	13	0.04	0.8
VH1	26	0.15	9.6	15	0.04	1.2

TABLE 4.6

Relative L^1 errors of vorticity and density shown in percentages and relative error shown in percentages of total kinetic energy (TKE) for the moving Gresho problem by all eight schemes on 80×20 and 160×40 grids.

	80×20 grid			160×40 grid		
Scheme	L^1 Vorticity error	L^1 Density error	Relative TKE error	L^1 Vorticity error	L^1 Density error	Relative TKE error
CFLFh	145	1.12	12.8	83	0.72	0.1
JT	100	0.81	42.8	52	0.22	22.1
LL	88	0.65	71.6	60	0.49	30.9
CLAW	65	0.72	39.9	37	0.29	8.3
WAFT	65	0.87	1.3	62	0.77	12.6
WENO	48	0.37	31.6	40	0.43	4.0
PPM	93	1.10	4.9	36	0.42	1.0
VH1	65	0.80	11.7	55	0.66	1.2

does improve much with the finer 160×40 grid. Regarding the vorticity error for the 160×40 grid, PPM and CLAW are the best. However, looking at Figure 4.11, one can note a rather large deviation from symmetry, as is also the case for most other schemes. Only JT keeps symmetry remarkably well.

5. Final remarks. We have taken a collection of schemes which are representative of most of the basic approaches to approximating the Euler equations by finite difference methods—including the use of central differencing, eigenvector decomposition, dimensional splitting, Runge–Kutta time stepping, limiting, hybridization, and Riemann solvers. We have applied these to a suite of problems in one and two dimensions. It is clear that some methods appear to work better than others on a specific problem, but no one scheme has shown itself to be superior on all of them, which should come as no surprise. Some schemes are much faster than others, but not too much should be read into this since in many cases we had to manipulate the data to fit into our framework.

We present this to the computational fluid dynamics community with the hope that it will contribute to the still vigorous research being done there. This paper presents selected results of the comparison. Results for all problems by all schemes are available on the website [31] including several animations of 2D test problems.

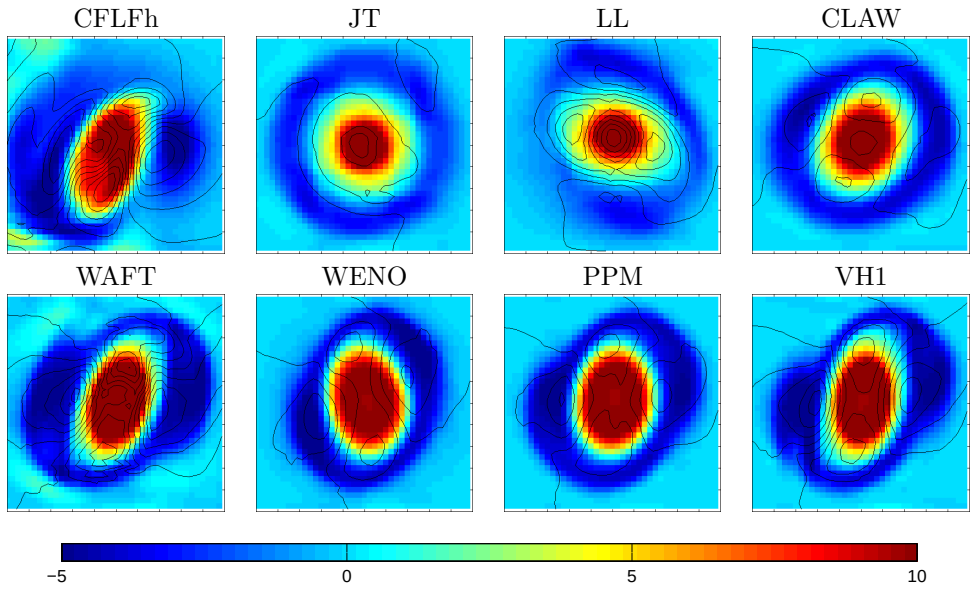

FIG. 4.11. *Results for the moving Gresho problem by all eight schemes on a* 160×40 *grid at time* $T = 3$ *in the square* $(x, y) \in (3, 4) \times (0, 1)$ *containing the vortex. Vorticity is displayed by color and density by* 11 *contours (from* 0.97 *to* 1.03 *with step* 0.006*). For initial exact vorticity see Figure* 4.10.

Acknowledgments. Many people have helped along the way in this project. Particular thanks are owed to Paul Woodward, who presented a careful appraisal of some of the problems and of the behavior of PPM. Eleuterio Toro generously shared with us the WAF code from the Numerica library. We also would like to acknowledge Mike Abouziarov, Tariq Aslam, Guan-Shan Jiang, Milan Kuchařík, Alexander Kurganov, Randall LeVeque, Xu-Dong Liu, Len Margolin, James Quirk, Misha Shashkov, Chi-Wang Shu, and Eitan Tadmor. R. Liska would like to thank the Institute for Geophysics and Planetary Physics (IGPP) of the Los Alamos National Laboratory for hosting his visits at Los Alamos National Laboratory. We also thank an anonymous referee for useful comments.

REFERENCES

[1] M. ABOUZIAROV, *On nonlinear amplification mechanism of instability near density discontinuities and shock waves for finite volume methods for Euler equations*, in HYP 2002, The Ninth International Conference on Hyperbolic Problems: Theory, Numerics and Applications, Abstracts, T. Hou and E. Tadmor, eds., Caltech, Pasadena, CA, 2002, p. 162.

[2] P. ARMINJON, D. STANESCU, AND M. VIALLON, *A two-dimensional finite volume extension of the Lax-Friedrichs and Nessyahy-Tadmor schemes for compressible flows*, in Proceedings of the 6th International Symposium on Computational Fluid Dynamics, Vol. 4, M. Hafez and K. Oshima, eds., Lake Tahoe, NV, 1995, pp. 7–14.

[3] T. ASLAM, *personal communication*, 2001.

[4] S. BILLETT AND E. TORO, *On WAF-type schemes for multidimensional hyperbolic conservation laws*, J. Comput. Phys., 130 (1997), pp. 1–24.

[5] J. BLONDIN, *VH-1: The Virginia Numerical Bull Session Ideal Hydrodynamics PPMLR*, http://wonka.physics.ncsu.edu/pub/VH-1/index.html.

[6] E. J. Caramana, D. E. Burton, M. J. Shashkov, and P. P. Whalen, *The construction of compatible hydrodynamics algorithms utilizing conservation of total energy*, J. Comput. Phys., 146 (1998), pp. 227–262.
[7] S. Chang, X. Wang, and C. Chow, *The space-time conservation element and solution element method: A new high resolution and genuinely multidimensional paradigm for solving conservation laws*, J. Comput. Phys., 160 (1999), pp. 89–136.
[8] P. Colella and P. Woodward, *The piecewise parabolic method (PPM) for gas-dynamical simulations*, J. Comput. Phys., 54 (1984), pp. 174–201.
[9] C. M. Dafermos, *Hyperbolic Conservation Laws in Continuum Physics*, Springer-Verlag, Berlin, 1991.
[10] E. Godlewski and P.-A. Raviart, *Numerical Approximation of Hyperbolic Systems of Conservation Laws*, Springer-Verlag, Berlin, 1996.
[11] P. Gresho, *On the theory of semi-implicit projection methods for viscous incompressible flow and its implementation via finite-element method that also introduces a nearly consistent mass matrix: Part* 2: *Applications*, Int. J. Numer. Methods Fluids, 11 (1990), pp. 621–659.
[12] J. Gressier and J. M. Moschetta, *Robustness versus accuracy in shock-wave computations*, Int. J. Numer. Methods Fluids, 33 (2000), pp. 313–332.
[13] J. Grove and V. Mousseau, *personal communication*, Los Alamos National Laboratory, Los Alamos, NM, 2000.
[14] H. Hanche-Olsen, H. Holden, and K. A. Lie, *Conservation Laws Preprint Server*, http://www.math.ntnu.no/conservation.
[15] A. Harten, *The artificial compression method for computation of shocks and contact discontinuities:* III. *Self adjusting hybrid schemes*, Math. Comp., 32 (1978), pp. 363–389.
[16] A. Harten, B. Engquist, S. Osher, and S. Chakravarthy, *Uniformly high-order accurate essentially non-oscillatory schemes* III, J. Comput. Phys., 71 (1987), pp. 231–303.
[17] W. Hui, P. Li, and Z. Li, *A unified coordinate system for solving the two-dimensional Euler equations*, J. Comput. Phys., 153 (1999), pp. 596–637.
[18] G.-S. Jiang and E. Tadmor, *Nonoscillatory central schemes for multidimensional hyperbolic conservation laws*, SIAM J. Sci. Comput., 19 (1998), pp. 1892–1917.
[19] G.-S. Jiang and C.-W. Shu, *Efficient implementation of weighted ENO schemes*, J. Comput. Phys., 126 (1996), pp. 202–228.
[20] S. Jin and Z. Xin, *The relaxation schemes for systems of conservation laws in arbitrary space dimensions*, Comm. Pure Appl. Math., 48 (1995), pp. 235–276.
[21] D. Kröner and M. Ohlberger, *A posteriori error estimates for upwind finite volume schemes for nonlinear conservation laws in multi dimensions*, Math. Comput., 69 (1999), pp. 25–39.
[22] M. Kuchařík, *personal communication*, 2001.
[23] A. Kurganov and E. Tadmor, *Solution of Two-Dimensional Riemann Problems for Gas Dynamics without Riemann Problem Solvers*, Technical report CAM 00-34, UCLA, Los Angeles, 2000.
[24] C. Laney, *Computational Gasdynamics*, Cambridge University Press, Cambridge, UK, 1998.
[25] P. D. Lax and X.-D. Liu, *Solution of two-dimensional Riemann problems of gas dynamics by positive schemes*, SIAM J. Sci. Comput., 19 (1998), pp. 319–340.
[26] R. LeVeque, *Numerical Methods for Conservation Laws*, Birkhauser-Verlag, Basel, 1990.
[27] R. J. LeVeque, *High-resolution conservative algorithms for advection in incompressible flow*, SIAM J. Numer. Anal., 33 (1996), pp. 627–665.
[28] R. LeVeque, *Wave propagation algorithms for multi-dimensional hyperbolic systems*, J. Comput. Phys., 131 (1997), pp. 327–353.
[29] R. LeVeque, *Clawpack Version* 4.0 *User's Guide*, Technical report, University of Washington, Seattle, 1999. Available online at http://www.amath.washington.edu/~claw/.
[30] R. Liska and B. Wendroff, *Composite schemes for conservation laws*, SIAM J. Numer. Anal., 35 (1998), pp. 2250–2271.
[31] R. Liska and B. Wendroff, *Comparison of Several Difference Schemes on* 1*d and* 2*d Test Problems for the Euler Equations*, Technical report, Czech Technical University, Prague, 2002. Available online with animations at http://www-troja.fjfi.cvut.cz/~liska/CompareEuler/compare8.
[32] X. Liu, *personal communication*, 2001.
[33] X. Liu and P. Lax, *Positive schemes for solving multi-dimensional hyperbolic systems of conservation laws*, Computational Fluid Dynamics Journal, 5 (1996), pp. 1–24. Available online at http://www.math.ucsb.edu/~xliu/publication/paper/positive1.pdf.
[34] K. W. Morton, *On the analysis of finite volume methods for evolutionary problems*, SIAM J. Numer. Anal., 35 (1998), pp. 2195–2222.

[35] H. Nessyahu and E. Tadmor, *Non-oscillatory central differencing for hyperbolic conservation laws*, J. Comput. Phys., 87 (1990), pp. 408–463.
[36] W. F. Noh, *Errors for calculations of strong shocks using an artificial viscosity and artificial heat flux*, J. Comput. Phys., 72 (1987), pp. 78–120.
[37] J. Quirk, *An Adaptive Grid Algorithm for Computational Shock Hydrodynamics*, Ph.D. thesis, College of Aeronautics, Cranfield University, Cranfield, UK, 1991. Available online at http://www.galcit.caltech.edu/~jjq/doc/amr_sol/thesis.
[38] J. Quirk, *A contribution to the great Riemann solver debate*, Int. J. Numer. Methods Fluids, 18 (1994), pp. 555–574.
[39] J. Quirk, *personal communication*, 2001.
[40] W. J. Rider, *Revisiting wall heating*, J. Comput. Phys., 162 (2000), pp. 395–410.
[41] P. J. Roache, *Computational Fluid Dynamics*, Hermosa Publishers, Albuquerque, NM, 1976.
[42] M. S. Sahota, P. J. O'Rourke, and M. C. Cline, *Assesment of Vorticity and Angular Momentum Errors in CHAD for the Gresho Problem*, Technical report LA-UR-00-2217, Los Alamos National Laboratory, Los Alamos, NM, 2000.
[43] C. W. Schulz-Rinne, J. P. Collins, and H. M. Glaz, *Numerical solution of the Riemann problem for two-dimensional gas dynamics*, SIAM J. Sci. Comput., 14 (1993), pp. 1394–1414.
[44] C. Shu and S. Osher, *Efficient implementation of essentially non-oscillatory shock-capturing schemes* II, J. Comput. Phys., 83 (1989), pp. 32–78.
[45] C. W. Shu and S. Osher, *Efficient implementation of essentially non-oscillatory shock-capturing schemes*, J. Comput. Phys., 77 (1988), pp. 439–471.
[46] J. Smoller, *Shock Waves and Reaction Diffusion Equations*, 2nd ed., Springer-Verlag, New York, 1994.
[47] G. A. Sod, *A survey of several finite difference schemes for hyperbolic conservation laws*, J. Comput. Phys., 27 (1978), pp. 1–31.
[48] G. Strang, *On the construction and comparison of difference schemes*, SIAM J. Numer. Anal., 5 (1968), pp. 506–517.
[49] E. Toro, *A weighted average flux method for hyperbolic conservation laws*, Proc. Roy. Soc. London Ser. A, 423 (1989), p. 401–418.
[50] E. Toro, *Riemann Solvers and Numerical Methods for Fluid Dynamics*, Springer-Verlag, Berlin, Heidelberg, 1997.
[51] E. Toro, *Numerica: A Library of Source Codes for Teaching, Research and Applications*, 2000. Available online at http://www.numeritek.com/numerica_software.html.
[52] P. Woodward and P. Colella, *The numerical simulation of two-dimensional fluid flow with strong shocks*, J. Comput. Phys., 54 (1984), pp. 115–173.
[53] P. Woodward, S. E. Anderson, D. H. Porter, I. Quesnell, M. Jacobs, and B. Edgar, *PPMLib Library*, University of Minnesota, Minneapolis, 1999. Available online at http://www.lcse.umn.edu/PPMlib/.